Power System Technology
Volume 49, No. 1, 2025
ISSN: 1000-3673

Synthesis of Kalman filter in quadcopter roll control loop based on PD-PI controller

Pham Trong Hai
Electrical Power Engineering Department, Tomsk Polytechnic University, Tomsk, Russian Federation
Shilin Alexander Anatolyevich
Electrical Power Engineering Department, Tomsk Polytechnic University, Tomsk, Russian Federation
Lyapunov Danil Yurievich
Electrical Power Engineering Department, Tomsk Polytechnic University, Tomsk, Russian Federation
Tomsk State University of Control Systems and Radioelectronics, Tomsk, Russian Federation
Shidlovskiy Stanislav Viktorovich
Department of Intelligent Technical Systems, Faculty of Innovative Technologies, Tomsk Polytechnic University, Tomsk, Russian Federation
Nguyen Minh Tuong
Department Informatics, MIREA – Russian Technological University; Moscow, Russian Federation

Abstract

Quadcopter attitude control using synchronous motors poses challenges for state estimation due to periodic disturbances caused by three-phase winding switching, which violate the standard Kalman filter's assumption of Gaussian noise. To address this, we propose a Kalman filter design that incorporates control signals and explicitly models these periodic disturbances. The filter is integrated into a roll and pitch angle control system using a modified PD-PI controller structure, which ensures compatibility between the control and estimation processes. Experimental validation on a real flight microcontroller, with implementation in C++, shows that the proposed filter reduces the variance of the estimated signals by a factor of four compared to standard approaches. Additionally, the system reveals that angle fluctuations at low speeds result from interactions between switching frequencies and controller discretization. These results demonstrate that the method enhances estimation accuracy and can be effectively applied to quadcopter platforms using both synchronous and asynchronous motors.

Keywords: Kalman filter, PID controller, roll control, synchronous motor, quadcopter

1. Introduction

In quadcopter flight control systems, one of the most technically demanding tasks is the stabilization of roll and pitch angles. These control loops exhibit second-order astatism [1], and their performance depends heavily on accurate state estimation using gyroscope and accelerometer data [2]. However, the raw measurements are affected by random noise [3] and mechanical disturbances [4] arising from motor characteristics and structural vibrations. To achieve high-quality control performance, it is essential to estimate angles, angular rates, and accelerations with minimal noise influence.

Most mass-market quadcopters rely on low-cost inertial measurement units (IMU), such as the MPU-6050, due to their compact size, affordability, low latency, and high sampling rates [4]. These sensors, while effective for basic motion tracking, exhibit characteristics such as Gaussian noise, zero drift over time [5], and limited computational precision. These limitations present specific challenges for embedded system design, where filtering and control algorithms must operate within strict memory and processing constraints.

Conventional filters often fall short in reducing interference and suppressing gyroscope noise [6], prompting the development of more advanced approaches [7]. Analysis of open-source flight controllers shows that complementary filters [8–9] and Kalman filters (KF) [10–11] are among the most widely adopted solutions. In KF-based implementations, dynamic models are typically expressed in matrix form with high-order difference equations, which require high numerical precision. As a result, most Python-based libraries [12] employ 64-bit floating-point arithmetic, making direct deployment to low-resource microcontrollers impractical.

Implementing advanced filtering on standard flight controllers, which often lack the computational power for full matrix operations [13–14], remains a significant challenge. Therefore, simplification of matrix-based filtering algorithms for embedded applications is a key focus of applied research [15]. Algebraic transformation of the KF equations enables lightweight implementations suitable for microcontrollers [16].

Another computational bottleneck in KF design lies in defining the covariance matrices Q and R, which are influenced by model adequacy and sensor noise. Their proper selection is critical for accurate estimation but also resource-intensive. Recent studies [17–18] have proposed evaluating the ratio of their determinants to simplify coefficient computation. Such approaches may significantly reduce onboard processing requirements.

This work proposes an algebraic-form Kalman filter tailored to a localized roll control loop that explicitly incorporates the control signal and models periodic disturbances. The KF coefficients are derived from the ratio of covariance matrix determinants to reduce computational load. The method is experimentally validated on a microcontroller-based laboratory setup under noisy conditions, with analysis focused on the impact of periodic components—arising from motor switching—on filter performance and control stability.

2. Design of a mathematical model and control signal for a quadcopter

2.1. Mathematical model of a quadcopter

In the inertial coordinate system, the angular positions of the quadcopter are defined as $\eta = [\phi, \quad \theta, \quad \psi]^T$. In the body-fixed coordinate system, the angular velocities are defined as $v = [p, \quad q, \quad r]^T$.The orientation of the quadcopter is described by a rotation matrix, which transforms vectors from the body frame to the inertial frame. These matrices are written as:

$$R(\phi,\theta,\psi) = \begin{vmatrix} C_\psi C_\theta & C_\psi S_\theta S_\phi - S_\psi C_\phi & C_\psi S_\theta C_\phi + S_\psi S_\phi \\ S_\psi C_\theta & S_\psi S_\theta S_\phi + C_\psi C_\theta & S_\psi S_\theta C_\phi - C_\psi S_\phi \\ -S_\theta & C_\theta S_\phi & C_\theta C_\phi \end{vmatrix} \quad (1)$$

The body-frame angular velocity ν (measured by gyroscopes) is rotated into the inertial frame via W:

$$\dot{\eta} = W^{-1}(\phi,\theta)v, \begin{vmatrix} \dot{\phi} \\ \dot{\theta} \\ \dot{\psi} \end{vmatrix} = \begin{vmatrix} 1 & S_\phi T_\theta & C_\phi T_\theta \\ 0 & C_\phi & -S_\phi \\ 0 & S_\phi/C_\theta & C_\phi/C_\theta \end{vmatrix} \begin{vmatrix} p \\ q \\ r \end{vmatrix} \quad (2)$$

The thrust and drag force generated by the i-th motor along the z-axis of the body-fixed frame is expressed as:

$$\begin{cases} f_i = K_e {\omega_i}^2 \\ M_i = K_d {\omega_i}^2 \end{cases} \quad (3)$$

where ω_i = rotational speed of the i-th rotor, K_e = thrust coefficient. K_d = drag coefficient.

The Newton-Euler equation for the quadcopter motion is described as follows:

$$\begin{cases} m\dot{V_B} = RF_i + F_d + F_g \\ v = W\dot{\eta} \\ M = J_M\dot{v} + v \times J_M v + \Gamma_g + \Gamma_a \end{cases} \quad (4)$$

где m = mass of the quadcopter; F_d, F_g – resultant drag force and gravitational force, Γ_g – torque due to gravity, Γ_a – resultant aerodynamic friction torque, J_M – moment of inertia tensor, calculated as:

$$J_M = \begin{vmatrix} I_{xx} & 0 & 0 \\ 0 & I_{yy} & 0 \\ 0 & 0 & I_{zz} \end{vmatrix}$$

The vector equation (5), along with the rotational equation, can be resolved into components along the three axes (x, y, z) as follows:

$$\begin{cases} \ddot{z} = \dfrac{F}{m}\left(C_\phi C_\theta\right) - \dfrac{K_{fz}}{m}\dot{z} - g, \\ \dot{\phi} = p + qS_\phi T_\theta + rC_\phi T_\theta, \\ \dot{\theta} = qC_\phi - rS_\phi, \\ \dot{\psi} = q\dfrac{S_\phi}{C_\theta} + r\dfrac{C_\phi}{C_\theta}, \\ \ddot{\phi} = \dfrac{1}{I_{xx}}\left((I_{yy} - I_{zz})\dot{\theta}\dot{\psi} - K_{ax}\dot{\phi} - J_r\dot{\theta}\Omega + \mathrm{M}_\phi\right), \\ \ddot{\theta} = \dfrac{1}{I_{yy}}\left((I_{zz} - I_{xx})\dot{\phi}\dot{\psi} - K_{ay}\dot{\theta} + J_r\dot{\phi}\Omega + \mathrm{M}_\theta\right), \\ \ddot{\psi} = \dfrac{1}{I_{zz}}\left((I_{xx} - I_{yy})\dot{\varphi}\dot{\theta} - K_{az}\dot{\psi} + \mathrm{M}_\psi\right). \end{cases} \quad (5)$$

3. Synthesis of kalman filter in roll control loop

In the complete quadcopter control system model [19], the control loops for pitch, roll, yaw, and vertical velocity can be separated. The control signal for all motors is generated through a mixing matrix that receives input values from each control loop with their respective signs and coefficients. As a result of this control loop separation, we obtain a linearized block diagram of the roll control loop shown in Figure. 2.

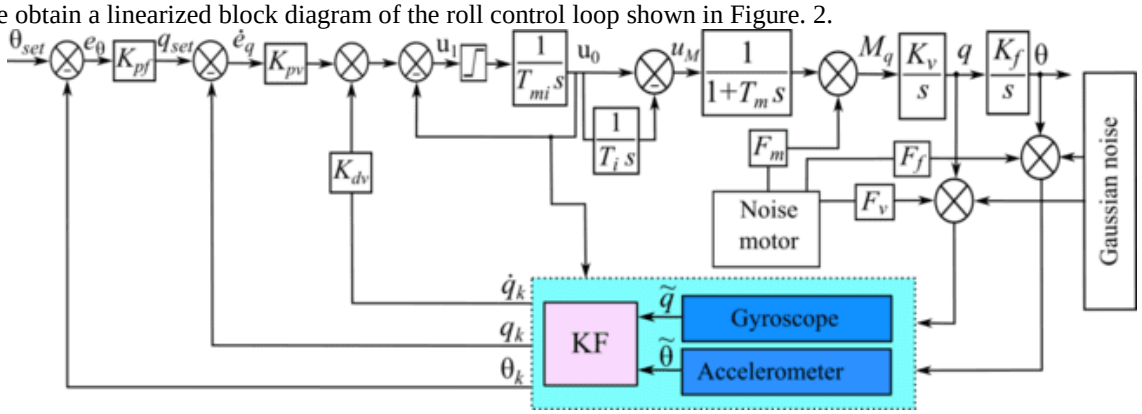

Figure 2. Structural diagram of the roll control circuit

Instead of a traditional PID controller, an equivalent PD-PI controller is used in the scheme. This configuration enables the use of a control signal u_0 centered around zero, since the actual signal u_M may contain a component compensating for quadcopter asymmetry. This component accumulates at the integrator output. The second reason for choosing this controller relates to enabling research on phase trajectory synthesis methods instead of linear dependence with parameters K_{pv} and K_{dv} in the PD control loop [20-21]. The roll control plant parameters are denoted as follows:

T_m – motor and converter inertia time;

K_v – relates roll torque to quadcopter angular rate;

K_f – establishes the relationship between angular rate and the angle itself, representing the gyroscope-accelerometer coupling parameter;

T_i – angular rate loop inertia time;

u_1 – control signal before the integrator;

M_q – angular acceleration torque.

Coefficients F_m, F_v, F_f are tuned such that spectral interference amplitudes match experimental results. This is because the rate sensor operates on the Coriolis effect, where acceleration compensation simultaneously dampens sensor housing vibration, resulting in vibrational noise amplitudes being lower than accelerometer values by comparison. The feedback integrator block with limiter maintains the control signal slew rate, defined by parameter T_{mi}. This eliminates low-frequency components in the interference signal spectrum during rapid motor speed changes [4].

According to the procedure for synthesizing the functional code for a linear system, seven steps should be performed in the control process, which are represented by the expressions:

$$
\begin{aligned}
&1)\ x_k = Fx_{k-1} + Bu \\
&2)\ P_k = FP_{k-1}F^T + Q \\
&3)\ \hat{y}_k = z_k - Hx_k \\
&4)\ S_k = HP_kH^T + R \\
&5)\ K_k = P_kH^TS_k^{-1} \\
&6)\ \hat{x}_k = x_k + K_k\hat{y}_k \\
&7)\ \hat{P}_k = (I - K_kH)P_k
\end{aligned}
\tag{18}
$$

Matrices *F*, *B*, *H* are determined by the control object and, according to the diagram in Figure. 1, are represented by differential equations

$$
\begin{aligned}
&\frac{\mathrm{d}\theta}{\mathrm{d}t} = qK_f; \\
&\frac{\mathrm{d}q}{\mathrm{d}t} = MK_v; \\
&\frac{\mathrm{d}M}{\mathrm{d}t} = \frac{u_M - M}{T_m}.
\end{aligned}
\tag{19}
$$

To obtain difference equations, we write them by replacing dt with the sampling interval, then expression (19) will take the form

$$
\begin{aligned}
&\frac{\theta_k - \theta_{k-1}}{\Delta t} = q_{k-1}K_f; \\
&\frac{q_k - q_{k-1}}{\Delta t} = M_{k-1}K_v; \\
&\frac{M_k - M_{k-1}}{\Delta t} = \frac{u - M_{k-1}}{T_M}.
\end{aligned}
\tag{20}
$$

Next, we express the state vector x_k and compose a matrix equation in expressions (18). Matrices *F*, *B*, *H* correspond to expressions:

$$
x_k = \begin{vmatrix} \theta_k \\ q_k \\ M_k \end{vmatrix}; x_{k-1} = \begin{vmatrix} \theta_{k-1} \\ q_{k-1} \\ M_{k-1} \end{vmatrix}; F = \begin{vmatrix} 1 & K_f\Delta t & 0 \\ 0 & 1 & K_v\Delta t \\ 0 & 0 & 1 - \frac{\Delta t}{T_M} \end{vmatrix}; B = \begin{vmatrix} 0 \\ 0 \\ \frac{\Delta t}{T_M} \end{vmatrix}; H = \begin{vmatrix} 1 & 0 & 0 \\ 0 & 1 & 0 \end{vmatrix}.
$$

Assuming that covariance matrices Q and R remain constant during control and characterize gyroscope angle/rate measurement quality along with model description accuracy, then steps 2, 4, 5, and 7 in expression (18) become independent of the plant's state variables. In this case, the Kalman Filter (KF) coefficient matrix can be studied separately from the control loop operation. Consequently, it suffices to analyze the ratio of absolute matrix determinants det(Q)/det(R) = ||Q|| / ||R|| when determining the KF coefficient matrix. The correspondence between det(Q)/det(R) values and the KF coefficient matrix is presented in table 1.

Table 1. Matrices of coefficients of the KF

det(Q)/det(R)	K_k	**det(Q)/det(R)**	K_k
0	$K_k = \begin{vmatrix} 0.00114 & 0.00028 \\ 0.00028 & 0.001 \\ 0 & 0 \end{vmatrix}$	∞	$K_k = \begin{vmatrix} 1 & 0 \\ 0 & 1 \\ 0 & 0.66 \end{vmatrix}$
10^{-3}	$K_k = \begin{vmatrix} 0.031 & 0.001 \\ 0.001 & 0.058 \\ 0.000074 & 0.011 \end{vmatrix}$	2.10^{-3}	$K_k = \begin{vmatrix} 0.044 & 0{,}001 \\ 0.001 & 0.075 \\ 0.0001 & 0.018 \end{vmatrix}$
0.02	$K_k = \begin{vmatrix} 0.13 & 0.0009 \\ 0.0009 & 0.176 \\ 0.0002 & 0.072 \end{vmatrix}$	0.2	$K_k = \begin{vmatrix} 0.36 & 0.00054 \\ 0.00054 & 0.4 \\ 0.00019 & 0.22 \end{vmatrix}$

After investigating several Kalman Filter (KF) implementation variants, it was determined that considering the ratio of absolute matrix determinants det(Q)/det(R).

• This ratio increases when greater model uncertainty and disturbances exist relative to measurement noise. In such cases, greater trust should be placed in measurement readings z_k.

• This ratio decreases when the plant model better matches the actual system while measurements exhibit significant noise. Here, greater confidence should be given to the plant model's state variables x_k.

For microcontroller implementation, matrix expressions 1, 3, and 6 in procedure (18) can be transformed into standard algebraic expressions for the following three filter execution steps:

$$\left.\begin{aligned}\theta_k &= \theta_{k-1} + K_{k\theta}\Delta t q_{k-1};\\ q_k &= q_{k-1} + K_{kq}\Delta t M_{k-1};\\ M_k &= M_{k-1} + \frac{\Delta t}{T_M}(u - M_{k-1});\end{aligned}\right\} (1)$$

$$\left.\begin{aligned}K_{k\theta} &= f_\theta(u_{pwm}, \mathrm{d}u/\mathrm{d}t);\\ K_{kq} &= f_g(u_{pwm}, \mathrm{d}u/\mathrm{d}t);\end{aligned}\right\} (2) \qquad (21)$$

$$\left.\begin{aligned}\hat{\theta}_k &= \theta_k + K_{k\theta}(z_\theta - \theta_k);\\ \hat{q}_k &= q_k + K_{kq}(z_\theta - q_k).\end{aligned}\right\} (3)$$

Kalman Filter (KF) coefficients are computed at the second step using the average motor power level u_{PWM} and the rate of change of the control signal du/dt through an approximating function $f_{k\theta,\,kq}(u_{PWM}, du/dt)$. This function adjusts KF coefficients $K_{k\theta}$ and K_{kq}. during abrupt motor transients, ensuring that during significant disturbances, the estimate relies more heavily on the control loop model than on gyroscope readings.

4. Simulation Results

According to the structure (Figure. 2), the control system can be divided into three nested loops, which are straightforward to tune (e.g. using modal optimization). For this reason, optimal loop tuning methods are not presented in this work.

Simulation results of the control loop without KF are shown in Figure. 3. The control signal u_M is less susceptible to noise due to the slew rate limiter between PD and PI elements. However, pronounced fluctuations in both control signal and angle are observed, linked to the discrepancy between sampling frequency and noise spectrum frequency. Such fluctuations are uncharacteristic of pure Gaussian noise. Similar fluctuations are visible in video materials accompanying this work [22], suggesting model adequacy when accounting for periodic vibrational interference in measurement channels.

The presence of such interference can be viewed not only as a gyroscope reading estimation problem but also as valuable information for detecting abnormal motor conditions. These include vibrations from propeller imbalance, damaged converter switches and motor winding faults. While this research direction extends beyond the article's scope, experimental results may benefit studies referenced in [23-26].

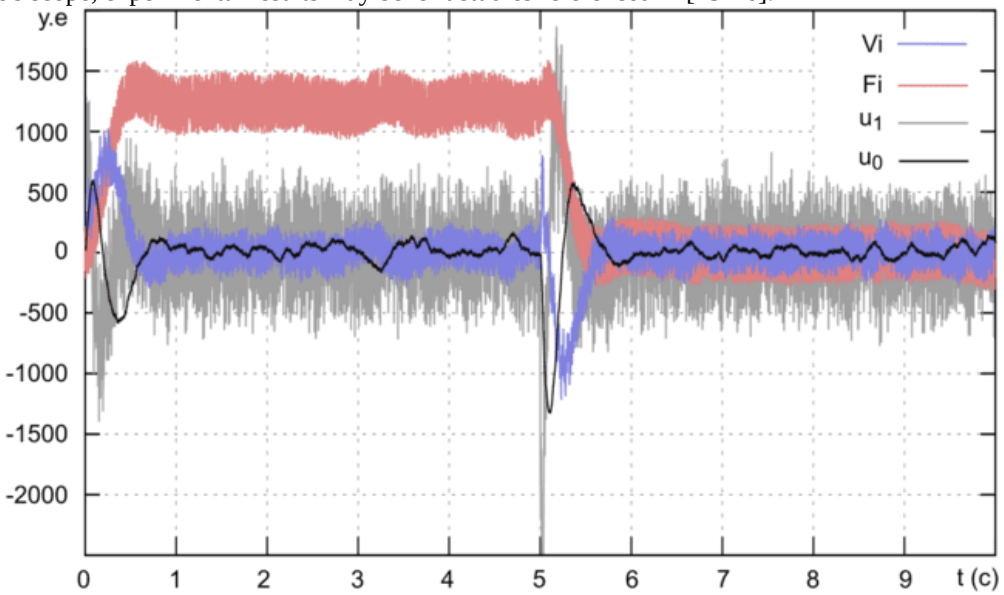

Figure 3. Simulation results with PD-PI controller without Kalman filter

The filter application (Figure. 4) enables higher-quality signals for the controller. The waveform of signal u_M now matches the derivative of signal kVi, such that dVi estimation can be performed with sufficient accuracy – critical for sliding mode control applications.

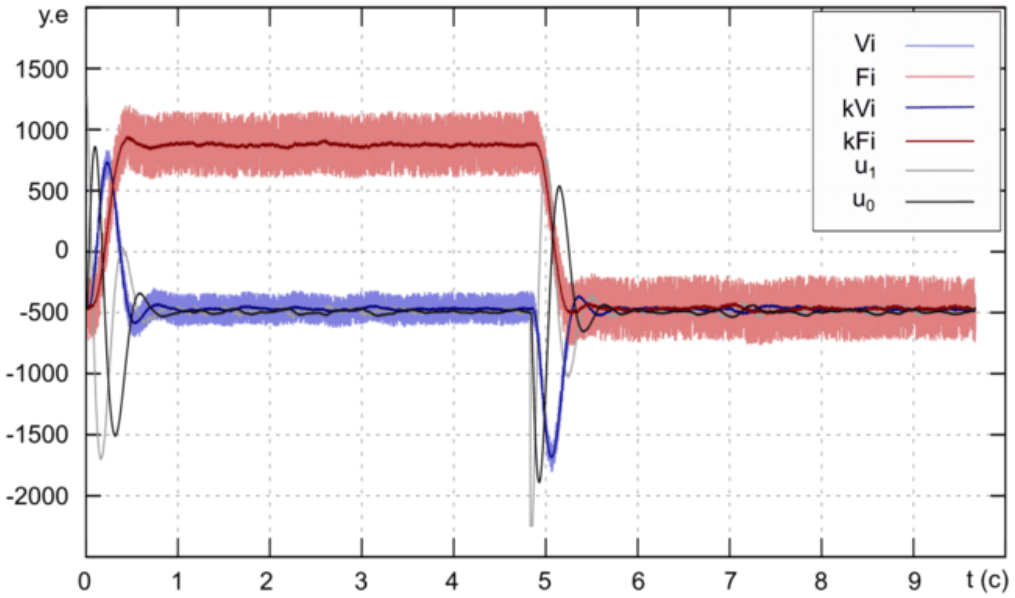

Figure4. Simulation results with PD-PI controller with Kalman filter

Analysis of the results shows that fluctuation is observed, but to a lesser extent. At the same time, the quality of the signals at the filter output is sufficient for studying control methods based on phase trajectories [20-21].

5. Experimental Setup and Results

A test bench was used to investigate the filter's performance. Video recordings and images of the experimental setup are available in the supplementary materials [22]. For performance comparison, we utilized open-source Kalman Filter (KF) code from public projects [27], which estimates roll angle only. Consequently, the transient process (Figure. 5a) displays solely measured and estimated roll angle values. The proposed filter's implementation is shown in Figure. 5b, featuring estimated angular rate signals. As seen in the figures, fluctuations persist in experimental results

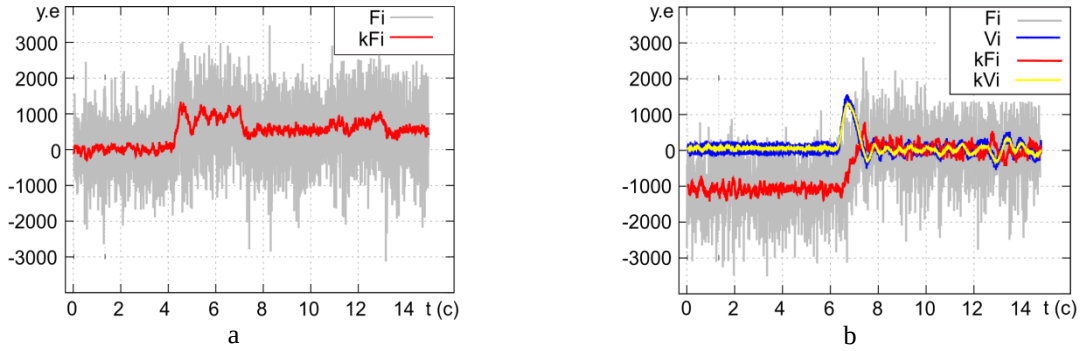

Figure5. Transient processes

To eliminate fluctuations in real control systems, signal averaging is typically employed. However, this approach extends transient processes beyond 2-3s. In our case, the transient duration is approximately one second, enabling investigation of time-optimal control methods for such applications.

In steady-state operation, the advantages of the proposed filter become visually apparent when observing set point angle maintenance [22]. Stabilization quality can be evaluated through transient analysis and by calculating estimated signal variances. Steady-state processes are shown in Figure. 6 (low motor speed, P_{PWM} = 25%) and Figure. 7 (high motor speed, P_{PWM} = 75%).

Experimental results show optimal KF coefficients ($K_{k\theta}$ = 0.13) and (K_{kq} = 0.18) correspond to det(Q)/det(R) = 0.02. According to table 1, the measurement channel's low-pass filter crossover frequency ($f_{kf} = K_{k\theta}/\Delta t$), with control loop sampling time ($\Delta t = 10^{-3}$ s), exceeds the periodic interference frequency range (60-80 Hz) and thus remains unfiltered.

Consequently, maximum fluctuation is observed in Figure. 6a at low RPM when using the Kalman filter implementation in BetaFlight.

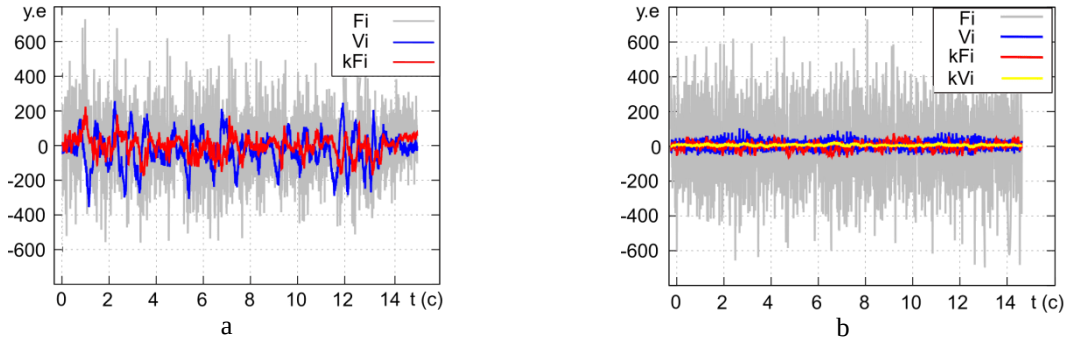

Figure 6. Steady-state processes at low engine speeds (20%)

This occurs because at low RPM, the periodic interference frequency is comparable to or lower than the measurement channel's inertial filter crossover frequency. The proposed filter estimates not only roll angle but also angular rate and acceleration by incorporating both control signals and the control loop's mathematical model. Consequently, fluctuations are significantly reduced, as demonstrated in Figure. 6b.

At high RPM (600-800 Hz interference frequency), the noise becomes filterable. Hence, fluctuation amplitudes are negligible and comparable for both filters (Figure. 7). However, oscillations appear in the proposed filter's angular rate output (kVi) when sampling frequency approaches the periodic interference frequency. This sampling rate was intentionally selected during experiments to highlight the effect.

These oscillations likely result from beating effects between motor interference and sampling frequencies. Direct frequency comparison for verification is challenging due to insufficient precision in measuring ESC rotational speeds. Physical validation would require a digital communication channel between ESCs and flight controllers to transmit actual phase-switching frequencies.

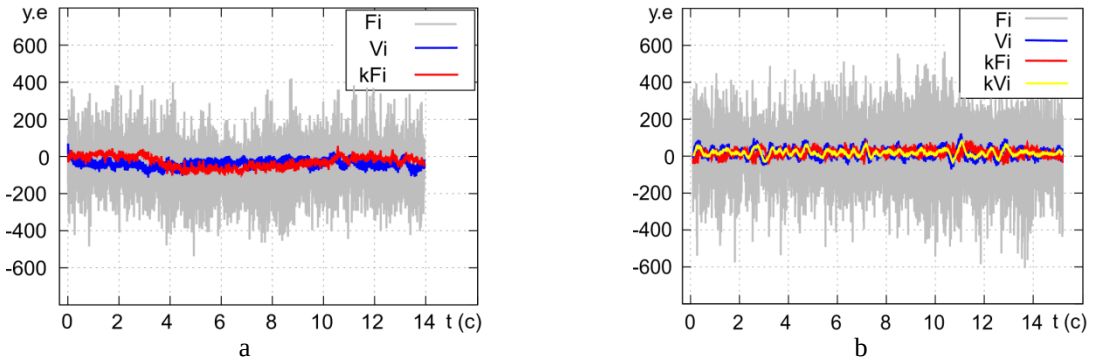

Figure 7. Steady-state processes at high engine speeds (75%)

For numerical evaluation, the results of calculating the variance ratios (output-to-input) are summarized in table 2. At high power, when the filter effectively suppresses vibrational noise, the proposed filter and the one used in the angle measurement channel (kFi) were expected to perform with roughly equal efficiency. However, the variance ratios differ by a factor of 2.5 in favor of the proposed filter. The difference in input and output variances for the angular rate channel (kVi) yields more modest results, which is due to the fact that the Vi (velocity) measurement channel has lower noise compared to the Fi (angle) measurement channel in the MPU-6050.

At low power, when the filter does not suppress vibrational noise, the performance of the proposed filter differs from that of the kFi channel filter by nearly a factor of 9, again favoring the proposed filter. This is due to the inclusion of the roll control loop model and the control signal u_0. Notably, the filter remains effective even when the vibrational noise is periodic and does not follow Gaussian distribution.

The table does not include the variance ratios for the estimated derivative of the velocity (kVi), which can be evaluated based on the measured Vi and the estimated kVi. This ratio is given by the expression:

$$\sigma^2(k\mathrm{d}Vi) / \sigma^2(\mathrm{d}Vi) = 613211/\ 5787963=0.106$$

and allows for obtaining a higher-quality derivative dq/dt with a variance nearly 10 times lower. Additionally, as previously noted, the waveform of u_M matches the derivative of the kVi signal, meaning u_0 can be used to estimate dq/dt. In this case, the variance ratio is given by:

$$\sigma^2(u_0) / \sigma^2(k\mathrm{d}Vi) = 0.001$$

significantly better, since the u_0 signal is computed virtually noise-free. However, practical implementation of kdVi signal estimation in the flight controller requires additional research and falls outside the scope of this paper.

Table 2. Estimation of variances in steady state

Variables	**Dispersion**	
	Suggested filter	**Another filter**
In steady state with high rotation speed (PPWM = 75%)		
σ2(kFi) / σ2(Fi)	0.00675	0.0182
σ2(kVi) / σ2(Vi)	0.229	–
In steady state with low rotation speed (PPWM = 20%)		
σ2(kFi) / σ2(Fi)	0.00757	0.0672
σ2(kVi) / σ2(Vi)	0.0226	–

6. Conclusion

Fluctuations in maintained roll angle are observable even at the simulation stage when periodic noise is introduced into the roll control loop's mathematical model (Figure. 2). Experimental results show this effect more distinctly at low motor RPM than at high RPM.

Using the mathematical model and roll control parameters in the proposed flight controller (FC), compared to conventional implementations, yields higher-quality estimates of angle, angular rate, and angular acceleration (Figure3) under conditions of Gaussian noise combined with spectral components from motor three-phase switching transients. Simulation results (Figure. 4) suggest the estimated signal quality is sufficient for modern control methods requiring angular acceleration estimates. Notably, the transient response of signal u_0 closely matches the estimated derivative signal's waveform while exhibiting extremely low variance.

Attempts to develop function approximations for FC coefficients that account for both control signal and its rate of change showed no significant advantages. This may be explained by the existing rate limiter in the ESC motor controller's control system, which likely suppresses low-frequency spectral components (undetected in experimental results). Using FC coefficients for det(Q)/det(R) = 0.02 produced optimal results. Variations of $K_{k\theta}$ and K_{kq} coefficients within ± 30% of optimal values caused no significant degradation in output signal estimation quality. Consequently, for roll control applications, steps 2, 4, 5, 7 of the standard filter procedure (18) for calculating $K_{k\theta}$ and K_{kq} can be replaced with fixed values at det(Q)/det(R) = 0.02.

The proposed filter can be implemented in quadcopter control systems employing high-speed or sliding mode techniques where precise estimation of angular derivatives and acceleration is required.

Acknowledgments

The research was carried out within the program "Priority-2030" of National Research Tomsk Polytechnic University and the project FEWM-2023-0014 of Tomsk State University of Control Systems and Radioelectronics.

References

[1] Zhao B., Yue D., Yang Y, “Robust attitude tracking control for a variable-pitch quadrotor with uncertainties,” International Journal of Adaptive Control and Signal Processing., vol. 38, no. 5, pp. 1878–1897, 2024. doi: https://doi.org/10.1002/acs.3779.

[2] R. C. Leishman, J. C. Macdonald, R. W. Beard and T. W. McLain, “Quadrotors and Accelerometers: State Estimation with an Improved Dynamic Model,” IEEE Control Systems Magazine., vol. 34. no. 1, pp. 28–41, 2024. doi: 10.1109/MCS.2013.2287362.

[3] Noordin.A., M. A. M. Basri, and Z. Mohamed, “Sensor fusion algorithm by complementary filter for attitude estimation of quadrotor with low-cost IMU,” Telkomnika (Telecommunication Computing Electronics and Control), vol. 16. no. 2, pp. 868–875, 2018. doi: https://doi.org/10.12928/telkomnika.v16i2.9020

[4] Khay. F. CH, Gun'ko A. M., Shilin A. A, “Study of the relationship between gyroscope readings and electromechanical processes of a brushless DC motor,” Electronic means and control systems. Proceedings of the International Scientific and Practical Conference, no. 1-1, pp. 338–341, 2024. (in Russian)

[5] Zhmud' V. A. A, “MPU6050 accelerometer and gyroscope: first power-up on STM32 and studying static readings,” Automation and software engineering, no. 3 (25), pp. 9–22, 2018. (in Russian)

[6] Guo H., Hong H, “Research on filtering algorithm of MEMS gyroscope based on information fusion,” Sensors, vol. 19, no. 16, pp. 3552, 2019.

[7] Allende-Peña J. M., Rodríguez-Paredes S. A., Salmerón-Quiroz B. B, “Control and signal filtering system for a quadcopter; analysis, comparison and implementation via low-cost IMU and microcontroller,” Ingeniería, investigación y tecnología, vol. 22, no. 2, 2021.doi: https://doi.org/10.22201/fi.25940732e.2021.22.2.015

[8] Benziane L. et al, “Attitude estimation and control using linearlike complementary filters: theory and experiment,” IEEE Transactions on Control Systems Technology, vol. 24, no. 6, pp. 2133–2140, 2016. doi: https://doi.org/10.1109/tcst.2016.2535382
[9] Marantos P., Koveos Y., Kyriakopoulos K. J, “UAV state estimation using adaptive complementary filters,” IEEE Transactions on Control Systems Technology, vol. 24, no 4, pp. 1214-1226, 2015.
[10] Khodarahmi M., Maihami V, “A review on Kalman filter models,” Archives of Computational Methods in Engineering, vol. 30, no. 1. pp. 727–747, 2023.
[11] Xiong J. J., Zheng E. H, “Optimal kalman filter for state estimation of a quadrotor UAV,” Optik, vol. 126, no. 21, pp. 2862–2868, 2015.
[12] Schreppel C. et al, “Implementation of a C Library of Kalman Filters for Application on Embedded Systems,”/ Computers, vol. 11, no. 11, pp. 165, 2022. doi: https://doi.org/10.3390/computers11110165
[13] Selezneva M. S., Neusypin K. A., Proletarsky A. V, “Navigation complex with adaptive non-linear Kalman filter for unmanned flight vehicle,” Metrology and Measurement Systems, vol. 26, no. 3, pp. 541–550, 2019
[14] Valade A. et al, “A study about Kalman filters applied to embedded sensors,” Sensors, vol. 17, no. 12, pp. 2810, 2017.
[15] Schmitz G. et al, “A simplified approach to motion estimation in a UAV using two filters,” IFAC-PapersOnLine, vol. 49, no. 30, pp. 325–330, 2016.
[16] Valenti R. G., Dryanovski I., Xiao J, “A linear Kalman filter for MARG orientation estimation using the algebraic quaternion algorithm,” IEEE Transactions on Instrumentation and Measurement, vol. 65, no. 2, pp. 467–481, 2015.
[17] Alfian R. I., Ma'arif A., Sunardi S, “Noise reduction in the accelerometer and gyroscope sensor with the Kalman filter algorithm,” Journal of Robotics and Control (JRC), vol. 2, no. 3, pp. 180–189, 2021. doi: https://doi.org/10.18196/jrc.2375
[18] Singh Y., Mehra R, “Relative study of measurement noise covariance R and process noise covariance Q of the Kalman filter in estimation,” IOSR Journal of Electrical and Electronics Engineering, vol. 10, no. 6, pp. 112–116, 2015.
[19] Chang Z., Chu H., Shao Y, “Quadrotor trajectory-tracking control with actuator saturation,” Electronics, vol. 12, no. 3, pp. 484, 2023 .doi: https://doi.org/10.3390/electronics12030484
[20] Shilin A.A., Bukreyev V.G., Perevoshchikov F.V, “Synthesis and implementation of the λ-approach of sliding control in the heat consumption system,” Scientific and technical bulletin of information technologies, mechanics and optics, vol. 22, no. 3, pp. 501–508, 2022. (in Russian). doi: 10.17586/2226-1494-2022-22-3-501-508
[21] Shilin A. A., Khay F. CH., Vong V. N, “Synthesis of Fuzzy-controller by second-order object with delay” Computer Science and Automation, vol. 23, no. 5, pp. 1505-1531, 2024 . (in Russian)
[22] Pham T.H, Shilin A.A, “Reasearh data for this article,”. URL: https://drive.google.com/drive/folders/1urIXeWcRN5Zcf2gr0X-JRZzt8nZhlK9g (date of access: 25.04.2025).
[23] Odnokopylov, G. I. , Bragin, A. D. Fault tolerant vector control of induction motor drive (Article number 012015) // IOP Conference Series: Materials Science and Engineering, 2014, vol. 66, no. 1, pp. 1-6.
[24] Odnokopylov, G. I., Rozaev, I. A, “Fault-tolerant control of switched-reluctance drive in emergency modes,” 2015 International Siberian Conference on Control and Communications (SIBCON) proceedings, Omsk, May 21-23. - Novosibirsk: IEEE Russia Siberia Section, pp. 1-6, 2015 (in Russian).
[25] Odnokopylov, G.I., Rozaev, I.A, “Algorithms of fault-tolerant sensorless vector control of switched-reluctance motor in electrical oil pump,” Bulletin of the Tomsk Polytechnic University, Geo Assets Engineering 331(5), pp. 208-218, 2020.
[26] Odnokopylov, G.I., Bukreev, V.G., Rozaev, I.A, “Research of fault-tolerant switched-reluctance motor of electrical oil pump,” Bulletin of the Tomsk Polytechnic University, Geo Assets Engineering 330(10), pp. 69-81, 2019
[27] Kristian S.L, “Kalman filter library”. URL: https://github.com/TKJElectronics/KalmanFilter (date of access: 25.03.2025).